Zuo-Bing Wu*

Hysteresis in three-dimensional multi-layer molecularly thin-film lubrication

https://doi.org/10.1515/zpch-2023-0220
Received February 1, 2023; accepted April 26, 2023; published online May 12, 2023

Abstract: For three-dimensional multi-layer molecularly thin-film lubrication system with elastic substrates, roles of hysteresis on tribological properties are investigated by using the multiscale simulation method. It is found that multiple stick-slip transitions with/without hysteresis loops appear in a sliding process and form a quasi-periodic progress with lattice distance. For the few-/multi-layer thin-film lubrication system, as the load increases, the hysteresis length monotonously increases/tends to keep constant. The hysteresis is mainly caused by the relaxation of metastable states of solid atoms in the elastic substrates, which delays the system back to its equilibrium states. In the quasi-periodic shearing progress, the effective elastic coefficients and the hysteresis lengths approximately remain unchanged, which reveals that although the hysteresis loops with the same lengths appear in the sliding process, the total systematic energy is still conserved. These findings not only provide a profound understanding of roles of hysteresis in the thin-film lubrication system but also show the effects of film layers and loads on the systematic tribological properties, which are of great significance for practical applications.

Keywords: friction; hysteresis; multiscale modeling; shear stress; thin-film lubrication.

1 Introduction

Thin-film lubrication, which describes the relative sliding of two solid substrates separated by a thin fluid film, plays a fundamental role in the development of advanced ultra-precision mechanical equipment and micro-machine [1, 2] and on the understanding lubrication mechanism of faults in earthquakes [3, 4]. It is a complex phenomenon on spatial and temporal scales that range from microscopic to macroscopic [5–7]. On one hand, at the interface, the fluid molecules are adsorbed and adhered to the solid surfaces of two substrates. The thin fluid film can protect the

***Corresponding author: Zuo-Bing Wu**, LNM, Institute of Mechanics, Chinese Academy of Sciences, Beijing 100190, China; and School of Engineering Science, University of Chinese Academy of Sciences, Beijing 100049, China, E-mail: wuzb@lnm.imech.ac.cn

surfaces from being damaged when the surfaces are sheared, and also reduce the friction force or friction coefficient of the system in comparing with that of the dry friction. The substrates make molecular contacts at relatively few asperities and undergo elastic deformation, plastic flow, etc. Based on the crystalline model, in which a mono-layer fluid film is confined between two solid walls composed of crystal atoms, the solid-liquid transitions of the film or the stick-slip processes of the system were identified [8, 9]. The nonlinear relationship between the static friction force and the load was found in depending on the structures of the surfaces and the coverage of the film [10]. For the multi-layer fluid film, it is found that the critical friction stress depends on the number of the molecular layers in the film due to the deviation of viscosity from continuum behaviors [11]. The rheological changes of confined fluid from its bulk behaviors, such as enhance of equivalent viscosity, formation of ordering structure and solid-liquid transition, were reported [12–14]. Since then, with the emphasis on fluid film behaviors confined between two rigid walls, the thin-film lubrication and its mechanism are understood very well in a series of theoretical analyses, numerical simulations, and experimental investigations [15–21]. On the other hand, it is clearly reasonable that thin-film lubrication contains a complicated interplay among multiple spatial scales from molecular to macroscale scale [22]. To understand the multiscale phenomena in the thin-film lubrication, some coarse-graining molecular models considering effects of the elasticity of substrates were proposed. A free-energy corrected hybrid atomistic and coarse-grained method for two-dimensional thin-film lubrication was developed [23]. A hybrid atomistic/continuum modeling for two-dimensional contact and dry friction between solid substrates was reported [24]. For three-dimensional contact, multiscale couplings of the molecular dynamics and the finite element method were developed [25–27]. Recently, a multiscale method to treat three-dimensional thin-film lubrication and account for effects of elastic substrates was established [28]. It can successfully predict the tribological properties of the thin-film lubrication system in a quasistatic shearing process under a wide range of conditions, and significantly reduce the computing time and increase the computational efficiency.

In tribological experiments with Atomic Force Microscopy (AFM), the emergence of the loop enclosed by the stress curves in the forward and backward motions is termed as the hysteresis phenomenon, which is a characteristic that may be found in many machine elements in common engineering use. The area of the hysteresis loop describes as the amount of energy dissipation in the slipping processes, and the stress averaged in one cycle of motion represents the amplitude of friction [29–32]. The hysteresis and dissipation in a quasistatic friction process were connected with the collective properties of the elastic instability suffered by the surfaces [33]. For the paper-to-paper friction, a correlation between the magnitude of friction hysteresis of the different papers and the total area of the raised fibers was found

[34]. In the rolling element system, it was found that the equivalent damping ratio at resonance is able to characterize the dynamics of systems exhibiting hysteretic friction [35]. However, from the general consideration based on the different temporal regime, the hysteresis may appear when the time taken to measure the friction force is less than that required for the system to attain a state of thermodynamic equilibrium, but not vice versa. Even if the computational time for the tribological system, i.e., the time taken to measure the friction force, is long enough, the system still cannot reach a state of thermodynamic equilibrium. Due to the metastable states in constrained thermodynamics [36], the hysteresis was described as being generated in the molecular simulations based on a biased configurational distribution rather than the Boltzmann distribution [37]. This will lead to that the hysteresis still appears in the numerical results of reversible slipping processes, where the total energy is conserved (i.e., the heat dissipation due to the internal friction of materials is ignored), and must be incorporated into a complete molecular picture of friction. Thus, the friction with hysteresis was considered as the natural result of configurational constraints that are inherent in the adsorbed layer [38] and the main feature in the fault transitions occurring in earthquakes and landslides [39–41]. However, to the best of our knowledge, roles of the hysteresis and effects of film layers and loads on the hysteresis behaviors in the three-dimensional thin-film lubrication with elastic substrates have not been reported.

In this paper, by applying the multiscale method, we investigate roles of hysteresis of the three-dimensional multi-layer molecularly thin-film lubrication with elastic substrates in a sliding process and show effects of the film layers and the loads on systematic tribological properties (the stiffness, the friction and the hysteresis) of the thin-film lubrication system. Section 2 describes the multiscale model of thin-film lubrication system and provides a quantitative measure of the hysteresis loop. The numerical results of the thin-film lubrication system with several film layers and under different loads, which are obtained by using the multiscale simulation method, are analyzed in Section 3. Finally, in Section 4, the conclusions and discussions are given.

2 Multiscale model of thin-film lubrication system

Figure 1 displays a schematic of the hybrid atomistic and coarse-grained treatment of the three-dimensional contact, which consists of two face-centered cubic (FCC) crystalline substrates and a molecularly thin film. The substrates connected with the top and bottom walls are divided into near and far regions, which are depicted by using the atomistic and coarse-grained descriptions, respectively. The coarse-grained far regions are covered with two finite-element meshes and connected to

the near regions of the substrates. Each finite-element mesh in Figure 1 consists of "local" tetrahedral elements, whose nodes coincide with a subset of solid substrate and wall atoms. The top and bottom walls are assumed to be rigid and to keep crystallographically aligned within the FCC (001) plane. The bottom wall remains stationary in the "laboratory" reference frame; the top wall can be shifted in the *x*-and *y*-directions. The top wall remains parallel with the bottom wall and serves as a handle by which the substrate can be manipulated. Its sliding distance in the *x*-direction is specified by the register α, which is defined as

$$x_i^t = x_i^b + \alpha a, \tag{1}$$

where x_i^t and x_i^b denote the lateral positions of atoms in the top and bottom walls, respectively. α is the distance in the unit of the lattice constant by which the top wall is displaced laterally with respect to the bottom wall. The total configurational energy of the hybrid system is then given by

$$\begin{aligned} U\left(\mathbf{r}^{N_f}, \mathbf{r}^{N_s'}, \mathbf{R}^{N_n}\right) = & \frac{1}{2}\sum_{i=1}^{N_f}\sum_{j\neq i}^{N_f} u_{ff}(r_{ij}) + \sum_{i=1}^{N_f}\sum_{j=1}^{N_s'} u_{fs}(r_{ij}) \\ & + \frac{1}{2}\sum_{i=1}^{N_s'}\sum_{j\neq i}^{N_s'} u_{ss}(r_{ij}) + \frac{1}{2}\sum_{i=1}^{N_s'}\sum_{j=1}^{N_s''} u_{ss}(r_{ij}) \\ & + \frac{1}{2}\sum_{i=1}^{N_w}\sum_{j=1}^{N_s''} u_{ss}(r_{ij}) + \sum_{e=1}^{N_e} N_a^e\left[\frac{1}{2}\sum_{j\neq i} u_{ss}(r_{ij})\right] \\ & + \sum_{e=1}^{N_e} N_q^e 3k_BT \ln\left[\hbar|D|^{1/6}/k_BT\right], \end{aligned} \tag{2}$$

where N_s' and N_s'' stand for the numbers of atoms in near and far regions of the substrates, respectively. The fluid-fluid and fluid-solid interactions are described in the first two terms in Eq. (2). The band of near region is sufficiently wide, so that fluid atoms do not interact with underlying atoms in the far region. The solid-solid interaction in near region atoms and the solid-solid interactions of near region atoms with far region atoms are denoted in the next two terms in Eq. (2). The solid-solid interaction between far region atoms and wall atoms is included in the fifth term in Eq. (2). It is noted that only one half of the interaction in the fourth/fifth term in Eq. (2) is accounted. The coarse-grained contribution in the next to last term in Eq. (2) effectively accounts for the other half of the interactions between underlying and near-region atoms/wall atoms. Based on the local harmonic approximation method, the missing contribution of enslaved atoms frozen in the coarse-graining process is compensated in the last term in Eq. (2). k_B is Boltzmanns constant, $\hbar$ is Plancks constant, and D is the 3D local dynamical matrix associated with the centroid atom. In each term, the pair interaction is taken to be shifted Lennard-Jones (12,6) potential

$$u_{ab}(r) = \begin{cases} \phi_{ab}(r) - \phi_{ab}(r_c), & \text{if} \quad r < r_c; \\ 0, & \text{if} \quad r \geq r_c, \end{cases} \tag{3}$$

where

$$\phi_{ab}(r) = 4\epsilon_{ab}[(\sigma/r)^{12} - (\sigma/r)^{6}], \quad ab = ff, fs, ss. \tag{4}$$

The effective diameter σ and range r_c are the same for all pairs. Only the depth ϵ_{ab} of the attractive well depends on the composition of the pair. Due to the periodic boundary in the x-direction, the film atoms, which move in and out the system, are thought to stay in the system during the sliding process.

To compute the thermomechanical properties we employ the analogue of the isothermal-isobaric ensemble and obtain the shear stress T_{zx} of the hybrid system

$$T_{zx} = T_{zx,ff} + T_{zx,fs} + T^1_{zx,ss} + T^2_{zx,ss} \tag{5}$$

where

$$\begin{aligned}
T_{zx,ff} &= \frac{1}{2A}\sum_{i=1}^{N_f}\sum_{j\neq i}^{N_f} <u'_{ff}(r_{ij})x_{ij}z_{ij}\Big/(r_{ij}L_z)>, \\
T_{zx,fs} &= \frac{1}{A}\sum_{i=1}^{N_f}\sum_{j=1}^{N'_s} <u'_{fs}(r_{ij})x_{ij}z_{ij}\Big/(r_{ij}L_z)>, \\
T^1_{zx,ss} &= \frac{1}{A}\sum_{i=1}^{N'^{,t}_s}\sum_{j\neq i}^{N'^{,b}_s} <u'_{ss}(r_{ij})x_{ij}z_{ij}\Big/(r_{ij}L_z)>, \\
T^2_{zx,ss} &= \frac{1}{2A}\sum_{i=1}^{N'^{,t}_s}\sum_{j\neq i}^{N'^{,t}_s} <u'_{ss}(r_{ij})x_{ij}z_{ij}\Big/(r_{ij}L_z)> \\
&\quad + \frac{1}{2A}\sum_{i=1}^{N'^{,b}_s}\sum_{j\neq i}^{N'^{,b}_s} <u'_{ss}(r_{ij})x_{ij}z_{ij}\Big/(r_{ij}L_z)> \\
&\quad + \frac{1}{2A}\sum_{i=1}^{N'_s}\sum_{j=1}^{N''_s} <u'_{ss}(r_{ij})x_{ij}z_{ij}\Big/(r_{ij}L_z)> \\
&\quad + \frac{1}{2A}\sum_{i=1}^{N_w}\sum_{j=1}^{N''_s} <u'_{ss}(r_{ij})x_{ij}z_{ij}\Big/(r_{ij}L_z)> \\
&\quad + \frac{1}{A}\sum_{e=1}^{N_e} N^e_a\left[\frac{1}{2}\sum_{j\neq i} < u'_{ss}(r_{ij})x_{ij}z_{ij}\Big/(r_{ij}L_z)>\right] \\
&\quad + \frac{1}{A}\sum_{e=1}^{N_e} N^e_q\left[\frac{k_BT}{2} < \frac{1}{|D|}\frac{\partial|D|}{\partial\alpha a}>\right],
\end{aligned} \tag{6}$$

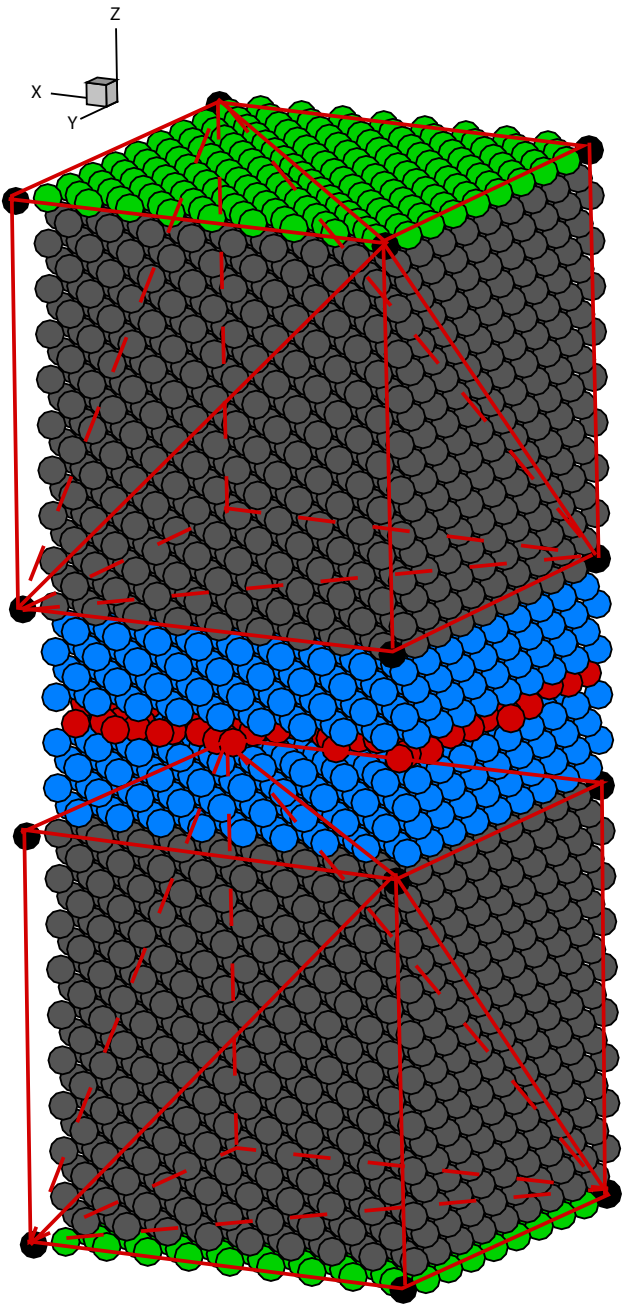

Figure 1: Schematic diagram of three-dimensional mono-layer molecularly thin-film lubrication system with periodic boundary conditions in $x-$ and $y-$ directions. The walls, the substrates and the fluid atoms are represented by solid green, blue and red spheres, respectively. The coarse grained far regions of the substrates are represented by solid dark gray spheres. All atoms are depicted in the configuration at $\alpha = 0$.

and $N_s^{',t}$ and $N_s^{',b}$ are the numbers of atoms in near regions of the substrate above and below the thin film, respectively. $T_{zx,ff}$, $T_{zx,fs}$, $T^1_{zx,ss}$ and $T^2_{zx,ss}$ are denoted as the shear stress of fluid-fluid atoms in the film, the shear stress of fluid-solid atoms near the surface, the shear stress of solid-solid atoms between upper and lower substrates and the shear stress of other solid-solid atoms in the system, respectively.

Figure 2 displays a schematic diagram of shear stress profiles of the thin-film lubrication in both the forward and backward directions, where exists a hysteresis loop. In general, the thin-film lubrication can undergo through multiple reversible processes and form multiple hysteresis loops. The hysteresis loop reflects the range of the same handle positions having the different shear stresses during the reversible processes.

A hysteresis length $l_{h,1t}$ of the loop in the first stick-slip transition of the thin-film lubrication is introduced to quantitatively depict the hysteresis phenomenon and defined as

$$\begin{aligned} l_{h,1t}/a &= \left[\alpha^f_{1t,b} - \alpha^f_{0e}\right] - \left[\alpha^b_{1t,a} - \alpha^f_{0e}\right] \\ &= \left[\alpha^f_{1t,b} - \alpha^f_{0e}\right] - \left[\alpha^f_{1e} - \alpha^f_{1t,a}\right] \\ &= \left[\alpha^f_{1t,b} - \alpha^f_{0e}\right] - \left[\left(\alpha^f_{0e} + 1\right) - \alpha^f_{1t,a}\right] \\ &= \alpha^f_{1t,b} + \alpha^f_{1t,a} - 2\alpha^f_{0e} - 1, \end{aligned} \tag{7}$$

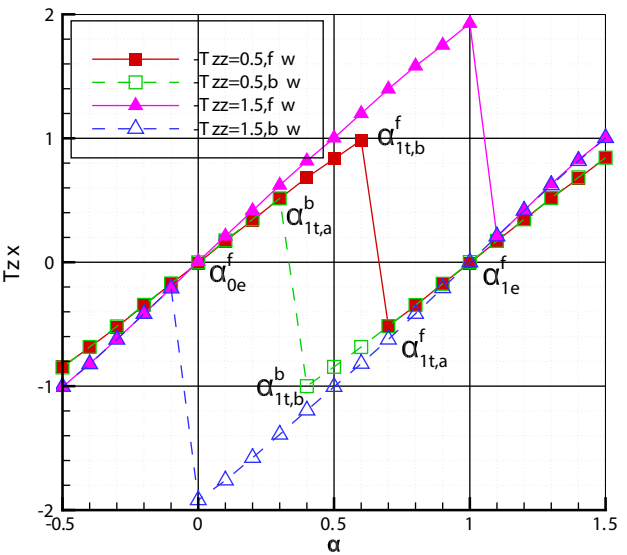

Figure 2: Schematic diagram of shear stress profiles of the thin-film lubrication under the loads $-T_{zz} = 0.5$ and 1.5. The forward and backward directions are encoded by solid and dished lines, respectively. The representative points (T_{zx}, α) for the forward/backward directions are represented by solid/open squares and deltas, respectively.

where $\alpha^f_{1t,b}$ and $\alpha^b_{1t,b}$ are the positions before the first slipping transition in the forward and backward directions, respectively. $\alpha^f_{1t,a}$ and $\alpha^b_{1t,a}$ are the positions after the first slipping transition in the forward and backward directions, respectively. $\alpha^f_{0e}/\alpha^f_{1e}$ is the initial/first equilibrium state of the system before/after the first slipping transition. For example, for $-T_{zz} = 0.5$ and $-T_{zz} = 1.5$ as shown in Figure 2, the hysteresis lengths in the first stick-slip transitions are $l_{h,1t}/a = \alpha^f_{1t,b} + \alpha^f_{1t,a} - 2\alpha^f_{0e} - 1 = 0.6 + 0.7 - 2 \times 0 - 1 = 0.3$ and $l_{h,1t}/a = \alpha^f_{1t,b} + \alpha^f_{1t,a} - 2\alpha^f_{0e} - 1 = 1 + 1.1 - 2 \times 0 - 1 = 1.1$, respectively. When the shearing process in the backward direction carries the system in reverse through precisely the same states as shearing in the forward direction, the hysteresis disappears, i.e., $l_{h,1t}$ is zero $\left(\alpha^b_{1t,a} = \alpha^f_{1t,b} = 0.5\right)$. Similarly, when the system undergoes multiple stick-slip transitions in the forward and backward directions, a hysteresis length $l_{h,nt}$ of the loop in the nth stick-slip transition is defined as

$$\begin{aligned} l_{h,nt}/a &= \left[\alpha^f_{nt,b} - \alpha^f_{(n-1)e}\right] - \left[\alpha^b_{nt,a} - \alpha^f_{(n-1)e}\right] \\ &= \left[\alpha^f_{nt,b} - \alpha^f_{(n-1)e}\right] - \left[\alpha^f_{ne} - \alpha^f_{nt,a}\right] \\ &= \left[\alpha^f_{nt,b} - \alpha^f_{(n-1)e}\right] - \left[\left(\alpha^f_{(n-1)e} + 1\right) - \alpha^f_{nt,a}\right] \\ &= \alpha^f_{nt,b} + \alpha^f_{nt,a} - 2\alpha^f_{(n-1)e} - 1 \\ &= \alpha^f_{nt,b} + \alpha^f_{nt,a} - 2\alpha^f_{0e} - 2n + 1, \end{aligned} \tag{8}$$

where $\alpha^f_{(n-1)e} = \alpha^f_{0e} + n - 1$. When $n = 1$, Eq. (8) returns to Eq. (7). In measuring the hysteresis loop in the nth stick-slip transition, the hysteresis length $l_{h,nt}$ is easier to calculate than the area of the hysteresis loop.

To account for effects of film atoms N_f on the tribological properties of the system, an integer of fluid layers in the film is defined as

$$n_f = N_f/N^c_s, \tag{9}$$

where N^c_s is FCC(001) surface atoms in substrates. The film layer n_f is limited between 1 and 5.

3 Numerical results

To compute the thermomechanical properties of the thin-film lubrication system under reversible shearing we perform isothermal-isobaric Monte Carlo (MC) simulations at a given atomistic number $N_f + N^{'}_s + N_n$, temperature T and normal stress $-T_{zz}$ [42]. Shearing process, which is regarded as a quasistatic, is performed by gradually increasing α in small increments $\Delta\alpha$. The initial film atoms are randomly placed between two solid surfaces at the register $\alpha = -0.5$. After M cycle MC running, the position, where the initial system forms an equilibrium state or not, depends on the atomistic layers n_f in the thin film. For the register $\alpha > -0.5$, the initial

configuration of the system is taken from the last configuration of the previous register $\alpha - \Delta\alpha$ combined with a linear increment ($0 \le \Delta x(z) \le \Delta\alpha$) of the several rows near the top wall. More details of the numerical methods can be found in [28]. Since the thin-film lubrication is a quasistatic reversible process, as shown in Figure 2, the shear stress profile in the backward process has the centro-symmetry with that in the forward process. In the following calculations, we only focus on the thermomechanical properties of the thin-film lubrication in the forward process ($\alpha = -0.5 \rightarrow 3$) and omit those in the backward process. Table 1 lists the values of the various parameters in the multiscale simulations. Numerical values are expressed in dimensionless units based on the Lennard-Jones parameters for the solid-solid interaction: distance is expressed in units of σ; energy in units of ϵ_{ss}; stress in units of ϵ_{ss}/σ; temperature in units of ϵ_{ss}/k_B.

3.1 Hysteresis in the mono-layer thin-film lubrication

We first investigate tribological behaviors of the mono-layer thin-film lubrication system ($n_f = 1$ or $N_f = 162$) at several loads $-T_{zz}$. Under certain load conditions, the fluid and solid atoms at the interface can form a FCC crystalline structure at the initial equilibrium state ($\alpha = 0$). In Figure 3(a), the system initially localized at $\alpha = -0.5$

Table 1: Parameters of the multiscale simulations of thin-film lubrication system.

Number of FCC(001) surface atoms in substrates $N_s^c = 162$
Number of top wall atoms $N_w^t = 162$
Number of bottom wall atoms $N_w^b = 162$
Number of atoms in a FCC cell $n_c = 4$
Total number of substrate atoms $N_s = 9 \times 9 \times 11 \times n_c \times 2 = 7128$
Number of near-region atoms $N_s^{'} = 9 \times 9 \times 2 \times n_c \times 2 = 1296$
Number of far-region atoms $N_s^{''} = 9 \times 9 \times 9 \times n_c \times 2 = 5832$
Number of local elements $N_e = 5 \times 2 = 10$
Number of nodes for local elements $N_n = 1 \times 2 = 2$
Density of substrate $\rho = 1.1$
Lattice constant of substrate $a = (\frac{4}{\rho})^{1/3} = 1.538$
Area of contact $A = L_x \times L_y = 9a \times 9a = 81a^2$
Temperature $T = 0.25$
Substrate-substrate Lennard-Jones depth $\epsilon_{ss} = 1$
Film-film Lennard-Jones depth $\epsilon_{ff} = 1/9$
Substrate-film Lennard-Jones depth $\epsilon_{sf} = 1/9$
Cutoff radius $r_c = 2.5$
Total number of Monte Carlo cycles $M \approx 10^5$

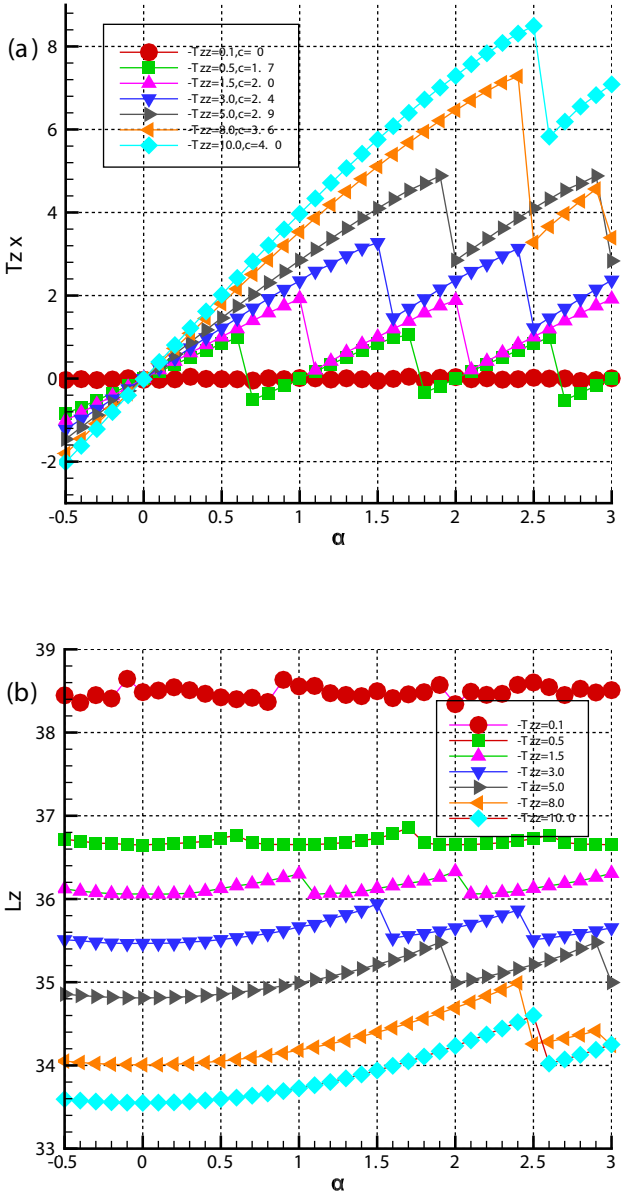

Figure 3: Tribological behaviors [(a) the shear stress profile (T_{zx} versus α) and (b) the mean separation profile (L_z versus α)] of the thin-film lubrication system with the film layer $n_f = 1$ (the film atoms $N_f = 162$) at the load $-T_{zz}$ = 0.1, 0.5, 1.5, 3, 5, 8 and 10, which are encoded by circle, square, delta, gradient, right and left triangles and diamond, respectively.

undergoes multiple stick-slip transitions in the range of $\alpha \in [-0.5, 3]$. From the initial equilibrium state ($\alpha = 0$), the appearance of the first stick-slip transition depends on the load, which affects the stiffness of the system by changing the intermolecular forces. After the first transition, the system forms a quasi-periodic stick-slip transition process with period a. In the sticking processes, the system may evolve through the first/second equilibrium state ($\alpha = 1/2$) or not, which depends on the load $-T_{zz}$. However, for a fixed load, the effective elastic coefficients ($c = \Delta T_{zx}/\Delta\alpha$) associated with shearing in the quasi-periodic sticking processes are approximately kept as a constant. In each slipping process, the shear stress T_{zx} abruptly changes from the local maximum to the local minimum and does not pass through any intermediate states between them. It corresponds to the quickly dropping of the average separation distance L_z in Figure 3(b). This phenomenon is denoted as the sharp transition.

At the smaller load ($-T_z = 0.1$), the system undergoes a free shearing process, where T_{zx} is almost zero. In the whole process, the thin film corresponds to the gaslike. When $-T_{zz} = 0.5$, the system passes through the initial equilibrium state ($T_{zx} = 0$) at $\alpha = 0$ in the sticking process to form a FCC crystalline structure, and slips in $\alpha = 0.6 \sim 0.7$. In the sticking process, the effective elastic coefficient c is 1.7. In the slipping process, system has a hysteresis loop with the length $l_{h,1t} = 0.3a$. After the slipping process, the system localized at $\alpha = 0.7$ goes back to the state of $\alpha = -0.3$. The snapshots of correspondent atomic configurations are drawn in Figure 4(a). At $\alpha = 0.6$, both the upper and the lower substrates tilt to the right with the same inclination. Their left boundaries approximately fit a straight line, i.e., the distances in the x-direction from the upper and lower solid surfaces to the straight line are almost equal. The fluid atoms are constrained in the cages composed of the solid atoms at the upper and the lower surfaces. The fluid and solid atoms in the interface are extruded in the FCC crystalline structure. At $\alpha = 0.7$, the solid atoms at the upper surface abruptly slip over the caged fluid atoms, so that the upper surface as a whole moves $0.5a$ to the right. Meanwhile, the whole lower surface with the thin-film atoms moves $0.5a$ to the left. Thus, the distance in the x-direction between the upper and the lower surfaces is approximately changed by the lattice distance a. The solid and fluid atoms tend to reform a FCC crystalline structure. In the sharp transition, as shown in Figure 4(c), the crystalline structure of the fluid atoms in the thin film is still kept. As the upper wall continuously moves to the right for the distance of $1.1a$ ($\approx a$), the system completes the second stick-slip transition. In the sticking process ($\alpha = 0.7 \sim 1.7$), the system passes through the first equilibrium state ($T_{zx} = 0$) at $\alpha = 1$ and keeps the effective elastic coefficient $c = 1.7$. In the slipping process ($\alpha = 1.7 \sim 1.8$), the system has a hysteresis loop with the length $l_{h,2t} = 0.5a(\approx l_{h,1t})$. After the slipping process, the system localized at $\alpha = 1.8$ goes back to the state of $\alpha = 0.8$ or -0.2. The snapshots of correspondent atomic configurations are drawn in

Figure 4(b). At $\alpha = 1.7$, both the upper and the lower substrates tilt to the right with the same inclination. The left boundaries of the upper and lower substrates approximately fit two parallel lines with the lattice distance a in the x-direction. The fluid atoms are constrained in the cages composed of the solid atoms at the upper and the lower surfaces, which forms an extruded FCC crystalline structure. At $\alpha = 1.8$, the solid atoms at the upper surface abruptly slip over the caged fluid atoms, so that the upper surface as a whole moves $0.5a$ to the right. Meanwhile, the whole lower surface with the thin film moves $0.5a$ to the left. Since the distance in the x-direction between the upper and lower solid surfaces is approximately changed by $2a$, the solid and fluid atoms in the interface tend to reform a FCC lattice structure. In the sharp transition, as shown in Figure 4(d), the crystalline structure of the fluid atoms in the thin film is still kept. As the upper wall moves to right for $0.9a$ $(\approx a)$, the system completes the third stick-slip transition. In the sticking process ($\alpha = 1.8 \sim 2.6$), the system passes through the second equilibrium state at $\alpha = 2$ and keeps the effective elastic coefficient $c = 1.7$. In the slipping process ($\alpha = 2.6 \sim 2.7$), the system has a hysteresis loop with the length $l_{h,3t} = 0.3a(= l_{h,1t})$. After the slipping process, the system localized at $\alpha = 2.7$ goes back to the state of $\alpha = 0.7$ or -0.3. The snapshots of correspondent atomic configurations (side/top view) are similar to those in the first or the second stick-slip transition.

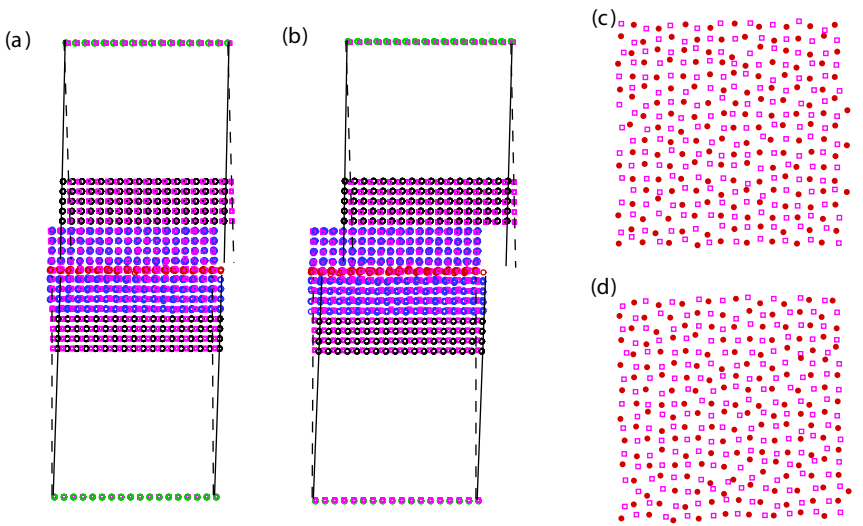

Figure 4: Whole atomistic structures (side view)/fluid atomistic structures (top view) of the stick-slip transitions in the tribological system with the film layer $n_f = 1$ (the film atoms $N_f = 162$) under the load $-T_{zz} = 0.5$ (a)/(c) at $\alpha = 0.6$ and 0.7 in the first transition and (b)/(d) at $\alpha = 1.7$ and 1.8 in the second transition. For the state ($\alpha = 0.6$ or 1.7)/($\alpha = 0.7$ or 1.8) before/after the transition, all atoms and the left boundaries of the substrates are denoted as in Figure 1/by the open pink squares and by the solid/dish lines, respectively.

As the load $-T_{zz}$ increases, the system undergoes a longer sticking process in the first stick-slip transition and slips at a larger α(>1). At the heavier load ($-T_{zz}$ = 3), as shown in Figure 3(a), the system passes through the initial equilibrium state (T_{zx} = 0) at α = 0, undergoes the sticking process in α = 0 ~ 1.5, and slips in α = 1.5 ~ 1.6. In the sticking process, the effective elastic coefficient c is 2.4. c is larger as the load $-T_{zz}$ increases, which reveals that the system loses partial elastic effects of both the upper and lower substrates. This property is also shown in Figure 3(b), where the average separation distance L_z decreases as the load $-T_{zz}$ increases. In the slipping process, system has a hysteresis loop with the larger length $l_{h,1t} = 2.1a$. The stronger hysteresis behavior is caused by the enhancement of stiffness of the system. After the slipping process, the system localized at α = 1.6 goes back to the state of α = 0.6. The snapshots of correspondent atomic configurations are described in Section A of Supplementary Information. As the upper wall moves to right, the system completes the second stick-slip transition. In the sticking process (α = 1.6 ~ 2.4), the system does not pass through the first equilibrium state (T_{zx} = 0) at α = 1, but keeps the effective elastic coefficient c = 2.4. In the slipping process (α = 2.4 ~ 2.5), the system has a hysteresis loop with the length $l_{h,2t} = 1.9a(\approx l_{h,1t})$. After the slipping process, the system localized at α = 2.5 goes back to the state of α = 0.5. The snapshots of correspondent atomic configurations are described in Section A of Supplementary Information.

To further investigate effects of the elements constituting the thin-film lubrication system on the maximal shear stress T^*_{zx} related to the hysteresis phenomena, T^*_{zx} in Eq. (5) and its components $T^*_{zx,ff}$, $T^*_{zx,fs}$, $T^{*1}_{zx,ss}$ and $T^{*2}_{zx,ss}$ in Eq. (6) are provided in Table 2. It reveals that at a given load $-T_{zz}$, the interaction $T^{*2}_{zx,ss}$ of the solid-solid atoms in the substrates contributes the main part of T^*_{zx}. The interaction $T^*_{zx,fs}$ of fluid-solid atoms near the surface has a little contribution to T^*_{zx}. Meanwhile, the contributions of both the interaction $T^*_{zx,ff}$ of fluid-fluid atoms in the film and the interaction $T^{*1}_{zx,ss}$ of solid-solid atoms between the upper and the lower substrates are close to zero. Therefore, the hysteresis in the thin-film lubrication system is mainly generated by the relaxation of metastable states of the solid atoms in the upper and lower substrates.

3.2 Hysteresis in the two-layer thin-film lubrication

Figure 5(a) displays the tribological behaviors of the two-layer thin-film lubrication system (n_f = 2 or N_f = 324) at several loads $-T_{zz}$. Under certain load conditions, both the fluid and solid atoms in the interface can form a FCC crystalline structure at the initial equilibrium state (α = −0.5). The system initially localized at α = −0.5 undergoes multiple stick-slip transitions in the range of $\alpha \in$ [−0.5, 3]. After the first stick-slip

Table 2: The maximal shear stress T^*_{zx} and its components $T^*_{zx,ff}$, $T^*_{zx,fs}$, $T^{*1}_{zx,ss}$ and $T^{*2}_{zx,ss}$ of the thin-film lubrication system with a film layer n_f (film atoms N_f) at a load $-T_{zz}$.

$n_f(N_f)$	$-T_{zz}$	$T^*_{zx,ff}$	$T^*_{zx,fs}$	$T^{*1}_{zx,ss}$	$T^{*2}_{zx,ss}$	T^*_{zx}
1(162)	0.5	−0.0003	−0.0198	−0.0009	1.07	1.0459
1(162)	1.5	0.0008	0.0739	0.0026	1.85	1.9167
1(162)	3.0	0.0013	0.1254	0.0034	3.15	3.2189
1(162)	5.0	0.0011	0.1738	0.0036	4.69	4.8715
1(162)	8.0	0.0013	0.2574	0.0008	7.02	7.2815
1(162)	10.0	0.0007	0.3001	−0.0023	8.19	8.4924
2(324)	1.5	0.0123	0.0218	−0.0002	0.49	0.5286
2(324)	3.0	0.0323	0.0602	0.0003	1.38	1.4768
2(324)	5.0	0.0533	0.1015	0.0009	2.48	2.6382
2(324)	8.0	0.0879	0.1712	−0.0003	4.35	4.6084
2(324)	10.0	0.1107	0.2159	−0.0007	5.57	5.8991

transition, the system forms a quasi-periodic transition process with the lattice distance a. In the sticking processes, the system may evolve through the first/second equilibrium state (α = 0.5/1.5) or not, which depends on the load. However, for a fixed load, the effective elastic coefficients c in the multiple sticking processes are approximately kept as a constant. In each slipping process, T_{zx} changes from the local maximum to the local minimum. However, there exists or not an intermediate state between them depending on the load. Meanwhile, the correspondent average separation distances L_z have different qualitative behaviors in Figure 5(b).

At the smaller load ($-T_{zz}$ = 0.5), the system undergoes a free slipping process, where T_{zx} is almost zero. In the whole process, the thin film corresponds to the gaslike. When the load $-T_{zz}$ = 1.5, the system firstly moves to α = −0.1 in a sticking process, and then slips in α = −0.1 ~ 0.1. The difference from the sharp transition is that there exists an intermediate state of $T_{zx} \approx 0$ at α = 0, where the thin film corresponds to the liquid. At the intermediate state, the average separation distance L_z is larger than those at its left and right neighbors (α = −0.1 and 0.1). This phenomenon is denoted as the smooth transition, where $l_{h,1t} = 0$ $\left(\alpha^f_{1t,b} = \alpha^f_{1t,a} = 0\right)$. After the slipping process, the system can arrive at the first equilibrium state (α = 0.5), i.e., the system localized at α = 0.5 goes back to the state of α = −0.5. In the stick-slip process, two processes in α = −0.5 ~ 0 and α = 0 ~ 0.5 have the centro-symmetry relative to α = 0, so the stick-slip process is precisely reversible. The system does not show hysteresis. The snapshots of correspondent atomic configurations are drawn in Figure 6(a). At α = −0.1, the upper and the lower substrates tilt to the right with the same inclination. Their left boundaries approach to two parallel lines with the

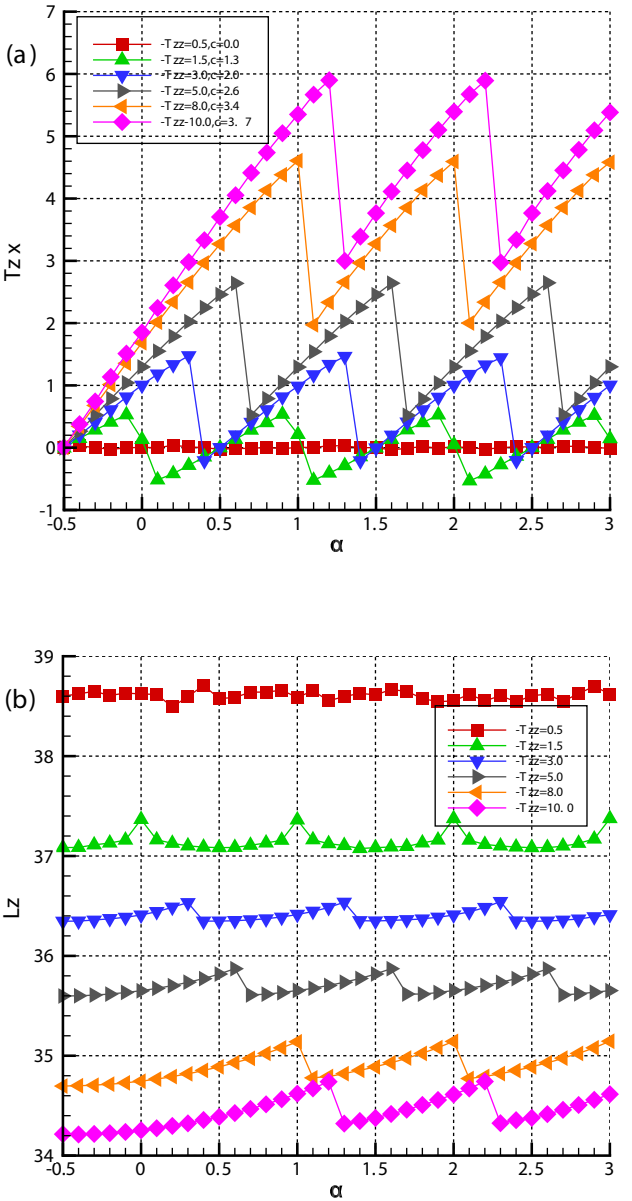

Figure 5: Same as Figure 3, except for the film layer $n_f = 2$ (the film atoms $N_f = 324$).

distance $0.25a$ in the x-direction. The fluid atoms are constrained in the cages composed of the solid atoms at the upper and the lower surfaces. The fluid and solid atoms at the interface are extruded to deviate from the FCC crystalline structure.

At $\alpha = 0$, the upper and the lower walls have the same x-coordinate. The upper and the lower substrates, which have the mirror-symmetry, cannot form a FCC crystalline structure with two layers of fluid atoms in the thin film. The thin film is liquid, so the shear stress $T_{zx} \approx 0$. The left boundaries of the upper and the lower substrates approximately fit a straight line. It corresponds to the local maximal average separation distance L_z. At $\alpha = 0.1$, the system completes the slipping process. The upper surface as a whole moves $0.5a$ to the right. Meanwhile, the whole lower surface moves $0.25a$ to the left. The upper surface is on the right of the lower one, but the distance in the x-direction between the upper and lower solid surfaces is about $0.5a$. In the smooth transition, as shown in Figure 6(c)–(d) and in Figure 7(a), the thin film moves away from the FCC crystalline structure and towards the liquid and finally reforms a FCC crystalline structure (the positions of fluid atoms in the upper/lower layer in the film after/before the sharp transition in Figure 6(d) and (c) can be interchanged with those in the lower/upper layer in the film before/after the sharp transition in Figure 6(c)/(d)). In the intermediate state at $\alpha = 0.0$, as shown in Figure 7(a), the crystalline structure of the fluid atoms in the thin film is partly lost (the fluid atoms are randomly distributed in some local zones). As the upper wall continuously moves to the right for the lattice distance a, the system completes the second stick-slip transition. Since the intermediate state with $T_{zx} \approx 0$ at $\alpha = 1$ exists in the slipping process ($\alpha = 0.9 \sim 1.1$), the stick-slip transition is still the smooth one. Similarly, in the shearing process, two processes in $\alpha = 0.5 \sim 1$ and $\alpha = 1 \sim 1.5$ have the centro-symmetry relative to $\alpha = 1$, so the stick-slip process is precisely reversible. The system has not any hysteresis loops. The snapshots of correspondent atomic configurations are drawn in Figure 6(b). At $\alpha = 0.9$, the upper and lower substrates tilt to the right with the same inclination. For convenience, in the following, the overall slipping distance with integer multiple of the lattice distance a in x-direction between the upper and lower substrates is ignored due to the periodicity in the FCC crystalline structure. The upper surface is on the left of the lower one. Their distance in the x-direction is about $0.25a$. Two layers of fluid atoms in the thin film confined by the upper and lower surfaces are extruded to deviate from the FCC crystalline structure. At $\alpha = 1$, the upper and lower substrates cannot form a FCC crystalline structure with two layers of fluid atoms in the thin film, so the thin film is liquid. In this case, the shear stress $T_{zx} \approx 0$ and the left boundaries of the upper and lower substrates approximately fit a straight line. The second local maximal average separation distance L_z appears in the system. At $\alpha = 1.1$, the system completes the slipping process between the upper and lower substrates. The upper surface as a whole moves $0.5a$ to the right. Meanwhile, the whole lower surface moves $0.25a$ to the left. The upper surface is on the right of the lower one, but the distance between the upper and lower solid surfaces in the x-direction is about $0.5a$. In the smooth transition, as shown in Figure 6(e)–(f) and in Figure 7(b), the thin film moves away from the FCC crystalline

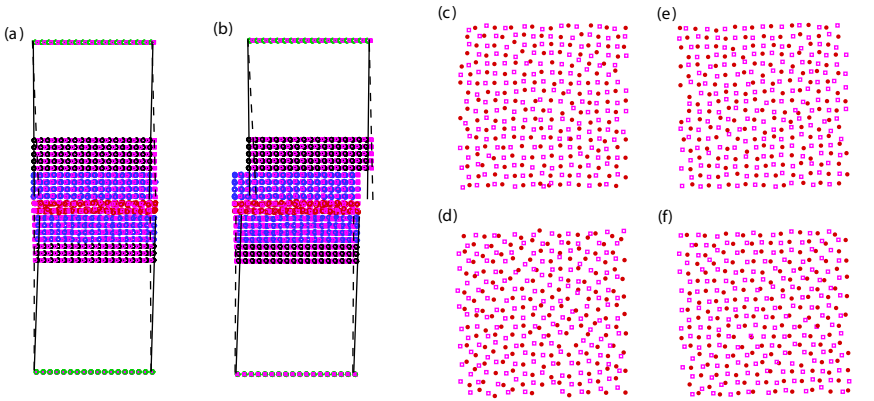

Figure 6: Whole atomistic structures (side view)/fluid atomistic structures of the [upper and lower] layers (top view) of the stick-slip transitions in the tribological system with the film layer $n_f = 2$ (the film atoms $N_f = 324$) under the load $-T_{zz} = 1.5$ (a)/[(c) and (d)] at $\alpha = -0.1$ and 0.1 in the first transition and (b)/[(e) and (f)] at $\alpha = 0.9$ and 1.1 in the second transition. For the state ($\alpha = -0.1$ or 0.9)/($\alpha = 0.1$ or 1.1) before/after the transition, all atoms and the left boundaries of the substrates are denoted as in Figure 1/by the open pink squares and by the solid/dish lines, respectively.

structure and towards the liquid and finally reforms the FCC crystalline structure. The positions of fluid atoms and their structures with the upper and lower solid surfaces in the second smooth transition are similar to those in the first smooth transition. As the upper wall moves to right for the lattice distance a, the system completes the third stick-slip transition. Since the intermediate state with $T_{zx} \approx 0$ at $\alpha = 2$ still exists in the slipping process ($\alpha = 1.9 \sim 2.1$), the stick-slip transition is still the smooth one. Similarly, in the shearing process, two processes in $\alpha = 1.5 \sim 2$ and $\alpha = 2 \sim 2.5$ have the centro-symmetry relative to $\alpha = 2$, so the stick-slip process is reversible. The system has no hysteresis. The sticking and slopping processes and correspondent atomic configurations are similar to those in the first or the second smooth transition.

As the load increases, the system undergoes a longer sticking process to complete the slipping at a larger α(>1). At the heavier load ($-T_{zz} = 5$), as shown in Figure 5(a), the system initially localized at $\alpha = -0.5$ as the initial equilibrium state ($T_{zx} = 0$) undergoes the sticking process in $\alpha = -0.5 \sim 0.6$ and then slips in $\alpha = 0.6 \sim 0.7$. In the sticking process, the effective elastic coefficient c is 2.6. c is larger as the load $-T_{zz}$ increases, which reveals that the system loses partial elastic effects of the substrates. This property is also shown in Figure 5(b), where the average separation distance L_z decreases when the load $-T_{zz}$ increases. In the slipping process, there does not exist an intermediate state ($T_{zx} = 0$), so the stick-slip transition is the sharp one. The slipping process is not precisely reversible. The hysteresis loop with the length

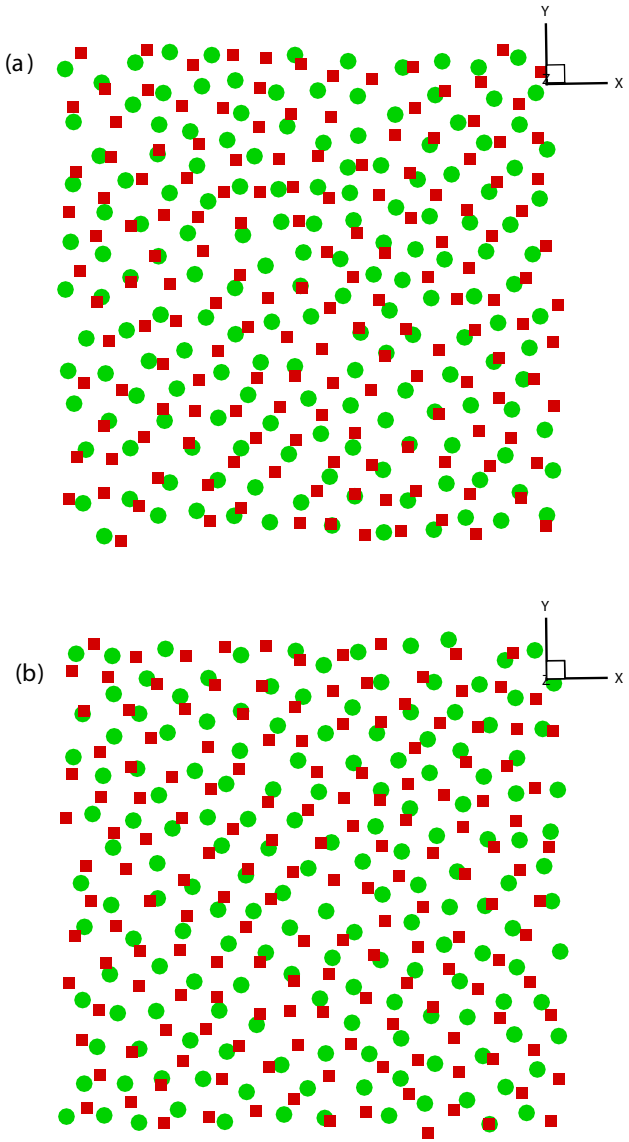

Figure 7: Fluid atomistic structures of the film (top view) of the stick-slip transitions in the tribological system with the film layer $n_f = 2$ (the film atoms $N_f = 324$) (a) at $\alpha = 0.0$ in the first transition under the load $-T_{zz} = 1.5$ and (b) at $\alpha = 1.0$ in the second transition under the load $-T_{zz} = 5$. The fluid atoms of the upper and lower layers in the film are denoted by the solid red squares and green circles, respectively.

$l_{h,1t}$ = 1.3a appears in the slipping process. The hysteresis behavior is caused by the enhancement of stiffness of the system. After the slipping process, the system localized at α = 0.7 goes back to the state of α = −0.3. The snapshots of correspondent atomic configurations are described in Section B of Supplementary Information. As the upper wall moves to right, the system complete the second stick-slip transition. In the sticking process in α = 0.7 − 1.6, the system does not pass through the first equilibrium states (T_{zx} = 0) at α = 0.5, but still keeps the effective elastic coefficient c = 2.6. The slipping process in α = 1.6 − 1.7 has a hysteresis loop with the length $l_{h,2t}$ = 1.3a(= $l_{h,1t}$). After the slipping process, the system localized at α = 1.7 goes back to the state at α = 0.7 or −0.3. The snapshots of correspondent atomic configurations are described in Section B of Supplementary Information. As the upper wall moves to right for the lattice distance a, the system completes the third stick-slip transition. The sticking and slopping processes and correspondent atomic configurations are similar to those in the first or second sharp transition.

Similarly, to further investigate effects of the elements constituting the thin-film lubrication system on the hysteresis, the maximal shear stress T^*_{zx} and its components related to the hysteresis are provided in Table 2. In comparison with the mono-layer thin-film lubrication system, the contributions $T^{*1}_{zx,ss}$ and $T^*_{zx,ff}$ of the interactions of the solid-solid atoms in the substrates and of the fluid-fluid atoms in the film are reduced and enhanced, respectively. However, the interaction $T^{*2}_{zx,ss}$ of the solid-solid atoms in the substrates is also the main part of T^*_{zx}. It reveals that the hysteresis of the thin-film lubrication is mainly generated by the relaxation of metastable states of the solid atoms in the substrates.

3.3 Tribological properties of the multi-layer fluid film lubrication system

In subsections 3.1 and 3.2, it is clear that the hysteresis properties of the thin-film lubrication are closely related to the stiffness and the friction properties of the system, which are described by the effective elastic coefficients c associated with shearing and the maximal shear stresses T^*_{zx}, respectively. In this subsection, by changing the load $-T_{zz}$ and the film layer n_f, we will investigate the systematic tribological properties of the multi-layer fluid film lubrication, which include the stiffness, the friction and the hysteresis of the system.

Figure 8 displays the tribological behaviors of the multiple-layer thin-film lubrication system (n_f = 3, 4, 5 or N_f = 486, 648, 810) at several loads $-T_{zz}$. For the odd/even layer film, under certain load conditions, the fluid and solid atoms in the interface can form a FCC crystalline structure at the initial equilibrium state

(α = 0/– 0.5). The system initially localized at α = –0.5 undergoes multiple stick-slip transitions in the range of $\alpha \in [-0.5, 3]$. In the multiple stick-slip transitions the system forms a quasi-periodic transition process with the period a. In the sticking processes, the system may pass through the first equilibrium states (α = 1/0.5) or not, which depends on the load. For a fixed load $-T_{zz}$, the effective elastic coefficients c in the multiple sticking processes are approximately kept as a constant. In the slipping processes, the shear stress T_{zx} changes from the local maximum to the local minimum. However, there exists or not an intermediate state between them depending on the load. With/without the intermediate state, the stick-slip transition is the smooth/sharp one. For the smooth/sharp transition, a hysteresis loop cannot/can be formed. At n_f = 3, the lighter load $-T_{zz} \leq 1.5$ corresponds to the smooth transition without the hysteresis loop, but the heavier load $-T_{zz} \geq 3$ corresponds to the sharp transition with the hysteresis loop. The critical load $-T_{zz}^* \in (1.5, 3)$ for classifying the smooth and the sharp transitions decreases as n_f increases from 3 to 5.

3.3.1 The effective elastic coefficient associated with shearing

The dependence of effective elastic coefficient c on the load $-T_{zz}$ and the film layer n_f represents the stiffness properties of the system. Figure 9(a) displays the effective elastic coefficient c versus the load $-T_{zz}$ at several film layers n_f. For a fixed film layer n_f, c monotonously increases as the load $-T_{zz}$ increases. When the load is heavier, the film is more compressed and hence the intermolecular forces that oppose the relative sliding of layers are stronger. For the film layer n_f = 1, since the stick-slip transition is always the sharp one, c starts at the load $-T_{zz}$ = 0.5 and linearly increases as the load $-T_{zz}$ increases. However, for the film layer $n_f \geq 2$, both the smooth and the sharp transitions may appear at the load $-T_{zz} > 0.5$, so the variation of c versus $-T_{zz}$ is divided into two stages. When $-T_{zz} \geq 3$, the stick-slip transition is the sharp one, so c almost linearly increases as $-T_{zz}$ increases. When $-T_{zz} < 3$, the stick-slip transition is the smooth one, so the variation of c versus $-T_{zz}$ is less than the linear growth. It reveals that for the few-layer thin-film lubrication under the wide range of load and the multi-layer thin-film lubrication under the heavier load, the heavier the load in the sticking process, the more compressed the film and consequently the stronger are the intermolecular forces that eventually forming of the harder film. The hard film with the two solid substrates approximately forms a whole FCC crystal with the almost identical stiffness. However, for the multi-layer thin-film lubrication under the lighter load, the load in the sticking process can only lead to form the softer film. The soft film with the two substrates cannot form a whole FCC crystal with the almost identical stiffness.

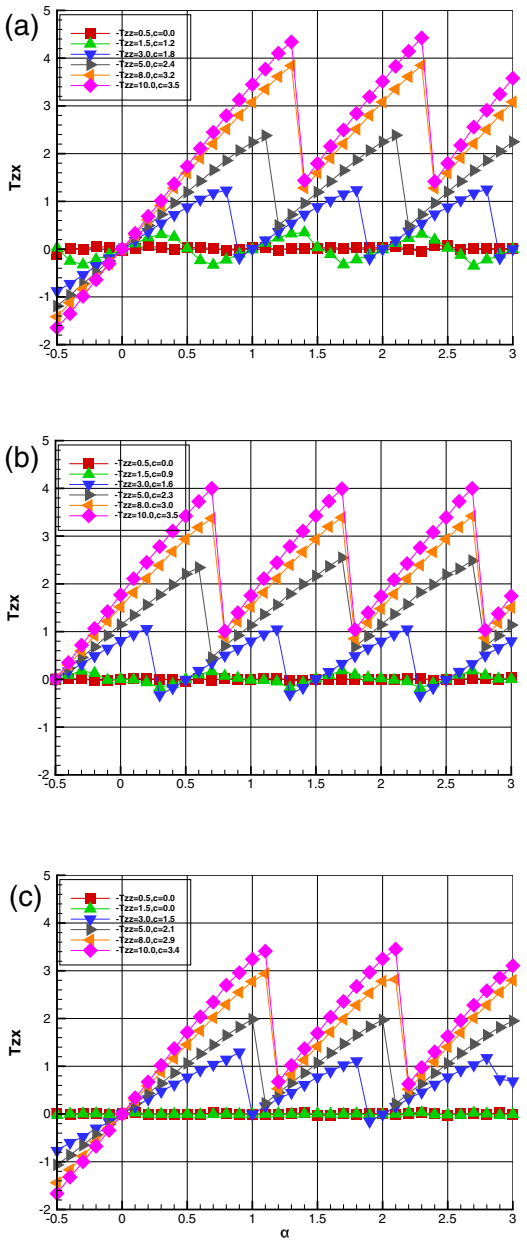

Figure 8: Shear stress profile (T_{zx} versus α) of the thin-film lubrication system with (a) the film layer $n_f = 3$ (the film atoms $N_f = 486$), (b) 4(648) and (c) 5(810) at the load $-T_{zz} = 0.5, 1.5, 3, 5, 8$ and 10, which are encoded by square, delta, gradient, right and left triangles and diamond, respectively.

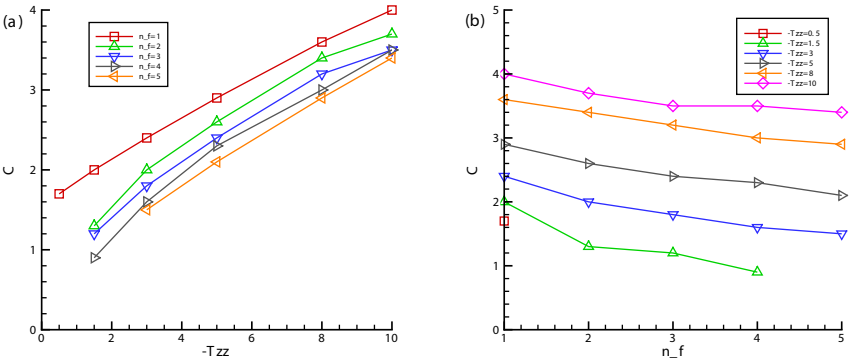

Figure 9: The effective elastic coefficient c associated with shearing versus (a) the load $-T_{zz}$ at the film layer n_f = 1, 2, 3, 4, 5 and (b) the film layer n_f at the load $-T_{zz}$ = 0.5, 1.5, 3, 5, 8, 10.

In Figure 9(b), at a fixed load $-T_{zz}$, the effective elastic coefficient c decreases as the film layer n_f increases. Since the interatomic forces within the film are weaker than those within the substrates, the system should become weaker as the proportion of film constituting it increases. When the load $-T_{zz} \geq 3$, c almost linearly and slightly decreases as n_f increases. When the load $-T_{zz} < 3$, c significantly decreases as n_f increases. It reveals that, at the lighter load, effects of the increasing film layer n_f on reducing the stiffness of the system in the sticking process are obvious. However, at the heavier load, the increase of the film layer n_f can only slowly reduce the stiffness of the system in the sticking process.

3.3.2 The maximal shear stress

The dependence of the maximal shear stress T^*_{zx} on the load $-T_{zz}$ and the film layer n_f represents the friction properties of the system. As shown in Figure 10(a), for the film layer n_f = 1 and 2, the maximal shear stress T^*_{zx} almost linearly rises as the load $-T_{zz}$ increases. The reason for this feature is the barrier to migration of film atoms confined in their effective cages is greater. The improved friction coefficient $\gamma = -\Delta T^*_{zx}/\Delta T_{zz}$ [28], which is independent of $-T_{zz}$, decreases as n_f increases. For the film layer n_f = 3, 4 and 5, since the barrier to migration of film atoms confined in their effective cages gradually decreases, the variation of T^*_{zx} versus $-T_{zz}$ is divided into two stages. In the range of $-T_{zz} < 5$, T^*_{zx} almost linearly increases as $-T_{zz}$ increases, so γ is a constant and independent of $-T_{zz}$. At a fixed load $-T_{zz}$, γ almost remains unchanged as n_f increases. However, in the range of $-T_{zz} \geq 5$, T^*_{zx} is not enough to achieve linear growth as $-T_{zz}$ increases, so γ depends on $-T_{zz}$. At a fixed load $-T_{zz}$, γ decreases as n_f increases. It

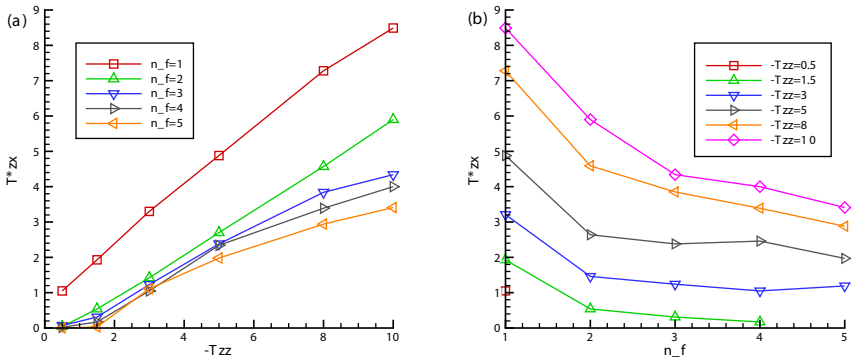

Figure 10: The maximal shear stress T^*_{zx} versus (a) the load $-T_{zz}$ at the film layer $n_f = 1, 2, 3, 4, 5$ and (b) the film layer n_f at the load $-T_{zz} = 0.5, 1.5, 3, 5, 8, 10$.

reveals that the friction properties for the few-layer thin-film lubrication under the wide range of load and the multi-layer thin-film lubrication under the lighter load are in accordance with the Amontons-Coulomb law for friction of unlubricated surfaces [47, 48], while the friction properties for the multi-layer thin-film lubrication under the heavier load deviates from the Amontons-Coulomb law for the friction of unlubricated surfaces.

Figure 10(b) displays curves of the maximal shear stress T^*_{zx} versus the film layer n_f at several loads $-T_{zz}$. In the range of $-T_{zz} \in [1.5, 5]$, T^*_{zx} significantly decreases when n_f increases from 1 to 2, but then T^*_{zx} approximately remains unchanged when n_f increases from 2 to 5. However, in the range of $-T_{zz} \in [8, 10]$, T^*_{zx} monotonously decreases as n_f increases. It reveals that, at the lighter load, effects of increasing the film layer in the range of $n_f \in [1, 2]/[3, 5]$ on reducing the maximal shear stress T^*_{zx} are obvious/invalid. However, at the heavier load, effects of increasing the film layer in the range of $n_f \in [1,2]/[3,5]$ on reducing the maximal shear stress T^*_{zx} are always significant.

3.3.3 The hysteresis length

The dependence of the hysteresis length $l_{h,it}$ on the load $-T_{zz}$ and the film layer n_f represents the hysteresis properties of the system. Figure 11(a) displays the hysteresis length $l_{h,1t}$ versus the load $-T_{zz}$ at several film layers n_f. For the film layer $n_f = 1$, the hysteresis loop appears at the load $-T_{zz} \geq 0.5$. It corresponds to that the sharp transition with the hysteresis loop can happen even under the lighter load for the mono-layer thin-film lubrication. For the film layer $n_f \geq 2$, the hysteresis loop disappears at the lighter load $-T_{zz} < 1.5$, but emerges at the heavier load $-T_{zz} \geq 1.5$. It

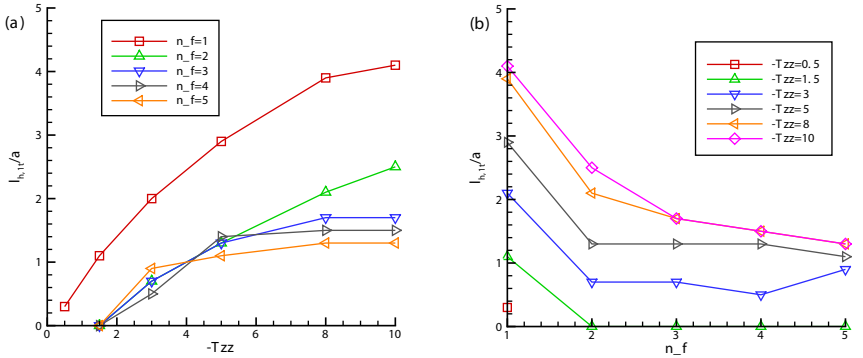

Figure 11: The hysteresis length $l_{h,1t}/a$ versus (a) the load $-T_{zz}$ at the film layer n_f = 1, 2, 3, 4, 5 and (b) the film layer n_f at the load $-T_{zz}$ = 0.5, 1.5, 3, 5, 8, 10.

shown that for the multi-layer thin-film lubrication, the smooth transition without the hysteresis loop remains under the lighter load, while the sharp transition with the hysteresis loop appears under the heavier load. Moreover, as the load $-T_{zz}$ increases, $l_{h,1t}$ monotonously increases for n_f = 1 and 2, while $l_{h,1t}$ initially monotonously increases and then keeps constant for n_f = 3, 4 and 5. It reveals that for the few-layer thin-film lubrication system, the elastic limit of the system always increases as the load increases. However, for the multi-layer thin-film lubrication system, the elastic limit of the system increases as the lighter load increases, but remains unchanged at the heavier load.

In Figure 11(b), for a fixed load $-T_{zz}$, the variation of the hysteresis length $l_{h,1t}$ with the film layer n_f has two stages. For the lighter load $-T_{zz} \leq 5$, $l_{h,1t}$ initially decreases and then approximately keeps constant as n_f increases. However, for the heavier load $-T_{zz} > 5$, $l_{h,1t}$ monotonously decreases as n_f increases. When the film layer $n_f \geq 3$, both the hysteresis lengths $l_{h,1t}$ for $-T_{zz}$ = 8 and 10 are the same, i.e., $l_{h,1t}$ keeps constant as the load $-T_{zz}$ increases. It reveals that, at a fixed load, the increasing film layer n_f to reduce hysteresis loop is obvious for the few-layer film ($n_f \in$ [1,2]), but is not obvious for the multi-layer film ($n_f \in$ [3,5]).

For the second and third stick-slip transitions, the hysteresis lengths $l_{h,2t}$ and $l_{h,3t}$ at a giving load $-T_{zz}$, which are determined by using Eq. (8), are almost equal to $l_{h,1t}$. Their hysteresis behaviors are similar to those for the first stick-slip transition.

4 Conclusions and discussions

Using the multiscale simulation method, we investigate roles of hysteresis in three-dimensional molecularly thin-film lubrication with elastic substrates during a

sliding process and show effects of film layers and loads on the systematic tribological properties including the stiffness, the friction and the hysteresis of the system. It is found that multiple stick-slip transitions with/without hysteresis loops appear in the sliding process and form a quasi-periodic progress with lattice distance. To quantitatively depict the hysteresis loop formed in the forward and backward shearing progresses, a hysteresis length in the first stick-slip transition is proposed and generalized to the multiple stick-slip transitions in the sliding process. For the few-/milti-layer thin-film lubrication system, as the load increases, the hysteresis length monotonously increases/tends to keep constant. In the thin-film lubrication system, the hysteresis is mainly caused by the relaxation of metastable states of solid atoms in the elastic substrates, which delays the system back to its equilibrium state.

In the quasi-periodic shearing progress, on one hand, the effective elastic coefficients are approximately kept as a constant. On the other hand, the hysteresis lengths in the multiple stick-slip transitions approximately remain unchanged. It reveals that although the hysteresis loops with the same lengths appear in the long sliding process, the total systematic energy is still conserved.

This study not only provides a profound understanding of the roles of hysteresis in the multi-layer thin-film lubrication system with elastic substrates, but also paves the way for optimizing the friction and the hysteresis, which are of great significance for practical applications [43–45] and to characterize the jamming transition of granular materials occurring in earthquakes and landslides [46].

Research funding: This research is supported by the National Natural Science Foundation of China through the Grants No. 11172310, No. 11472284 and No. 12272384. The author thanks the National Supercomputing Center in Tianjin for assisting in the computation.

Conflict of interest statement: The author declares no conflicts of interest regarding this article.

Data availability: The data that support the findings of this study are available from the corresponding author upon reasonable request.

Author contributions: The author has accepted responsibility for the entire content of this submitted manuscript and approved submission.

References

1. Bhushan B. *Tribology Issues and Opportunities in MEMS*; Springer: Berlin, 1998.
2. Luo J. B., Hu Y. Z., Wen S. Z. *Physics and Chemistry of Micro-/Nanotribology*; ASTM Inter: Maryland, 2008.
3. Bowden F. P., Tabor D. *The Friction and Lubrication of Solids*; Clarendon Press: Oxford, 1950.

4. Toro G. D., Hirose T., Nielsen S., Pennacchioni G., Shimamoto T. Natural and experimental evidence of melt lubrication of faults during eqrthquakes. *Science* 2006, *311*, 657–9.
5. Adamson A. W. *Physical Chemistry of Surfaces*, 3rd ed.; Wiley: New York, 1976.
6. Szeri A. Z. *Fluid Film Lubricantion*, 2nd ed.; Cambridge Uni. Press: Cambridge, 2012.
7. Gnecco E., Meyer E. *Elements of Friction Theory and Nanotribology*; Cambridge Uni. Press: Cambridge, 2015.
8. Schoen M., Rhykerd C. L., Diestler D. J., Cushman J. H. Shear forces in molecularly thin films. *Science* 1989, *245*, 1223–1225.
9. Thompson P. A., Robbins M. O. Origin of stick-slip motion in boundary lubrication. *Science* 1990, *250*, 792–795.
10. Gao G. T., Zeng X. C., Diestler D. J. Nonlinear effects of physisorption on static friction. *J. Chem. Phys.* 2000, *113*, 11293–11296.
11. Israelachvili J. N., Mcguiggan P. M., Homola A. M. Dynamic properties of molecularly thin liquid films. *Science* 1988, *240*, 189–191.
12. Luo J., Wen S., Huang P. Thin-film lubrication. Part I. study on the transtion between EHL and thin film lubrication using a relative optical interference intensity technique. *Wear* 1996, *194*, 107–115.
13. Hu Y. Z., Wang H., Guo Y., Zheng L. Q. Simulation of lubrication rheology in thin film lubrication part 1: simulation of poiseuille flow. *Wear* 1996, *196*, 243–248.
14. Tanner R. I., Jabbarzadeh A. Thin-film lubrication nano-rheology via molecular dynamics. *Australian J. Mech. Eng.* 2008, *5*, 43–50.
15. Yamada S. Nanotribology of symmetric and asymetric liquid lubricants. *Symmetry* 2010, *2*, 320–345.
16. Dong Y., Li Q., Martini A. Molecular dynamics simulation of atomic friction: a review and guide. *J Vac. Sci. Tech. A* 2013, *31*, 030801.
17. Krylov S. Y., Frenken J. W. The physics of atomistic-scale friction: basic considerations and open questions. *Phys. Status Solidi B* 2014, *251*, 711–736.
18. Ghaffari M. A., Zhang Y., Xiao S. Molecular dynamics modeling and simulation of lubricant between sliding solids. *J. Micromech. Mol. Phys.* 2017, *2*, 1750009.
19. Chen W., Amann T., Kailer A., Rühe J. Thin-film lubrication in the Water/Octyl β-D-Glucopyranoside system: macroscopic and nanoscopic tribological behavior. *Langmuir* 2019, *35*, 7136–7145.
20. Ahmed H., Biancofiore L. A new approach for modeling viscoelastic thin film lubrication. *J. Non-Newton Fluid Mech.* 2021, *292*, 104524.
21. Tang S., Li S., Ma L., Tian Y. Photorheological fluids of azobenzene polymers for lubrication regulation. *Friction* 2022, *10*, 1078–1090.
22. Vakis A. I., Yastrebov V. A., Scheibert J., Nicola L., Dini D., Minfray C., Almqvist A., Paggi M., Lee S., Limbert G., Molinari J., Anciaux G., Aghababaei R., Echeverri Restrepo S., Papangelo A., Cammarata A., Nicolini P., Putignano C., Carbone G., Stupkiewicz S., Lengiewicz J., Costagliola G., Bosia F., Guarino R., Pugno N., Müser M., Ciavarella M. Modeling and simulation in tribology across scales: an overview. *Tribol. Inter.* 2018, *125*, 169–199.
23. Wu Z.-B., Diestler D. J., Zeng X. C. Multiscale treatment of thin-flim lubrication. *Mol. Simul.* 2005, *31*, 811–815.
24. Luan B., Hyun S., Molinari J. F., Bernstein N., Robbins M. O. Multiscale modeling of two-dimensional contacts. *Phys Rev. E* 2006, *74*, 046710.
25. Pearson J. D., Gao G., Zikry M. A., Harrison J. A. Nanoindentation of model diamond nanocomposites: hierarchical modelcular dynamics and finite-element simulatrions. *Comput. Mater. Sci.* 2009, *47*, 1–11.
26. Ramisetti S. B., Aniaux G., Molinari J.-F. MD/FE multiscale modeling of contact. In *Fundamentals of Friction and Wear on the Nanoscale*; Gnecco E., Meyer E., Eds. Springer International Publishing: Switzerland, 2015; p. 289.

27. Savio D., Fillot N., Vergne P., Hetzler H., Seemann W., Espejel G. A multiscale study on the wall slip effect in a ceramic-steel contact with nanometer-thick lubricant film by a nano-to-elastohydrodynamic lubrication approach. *J. Tribol.* 2015, *135*, 031502.
28. Wu Z.-B. Multiscale simulation of three-dimensional thin-film lubrication. *Friction* 2021, *9*, 471–487.
29. Yoshizawa H., Chen Y. L., Israelachvili J. Fundamental mechanisms of interfacial friction. 1. Relation between adhesion and friction. *J. Phys. Chem.* 1993, *97*, 4128–4140.
30. Göddenhenrich T., Müller S., Heiden C. A lateral modulation technique for simultaneous friction and topography measurements with the atomic force microscope. *Rev. Sci. Instr.* 1994, *65*, 2870–2873.
31. Crassous J., Charlaix E., Loubet J. L. Nanoscale investigation of wetting dynamics with a surface force apparatus. *Phys. Rev. Lett.* 1997, *78*, 2425–2428.
32. Carpick R. W., Salmeron M. Scratching the surface: fundamental investigations of tribology with atomic force microscopy. *Chem. Rev.* 1997, *97*, 1163–1194.
33. Bocquet L., Jensen H. Phenomenological study of hysteresis in quasistatic friction. *J. Phys. I France* 1997, *7*, 1603–1625.
34. Garoff N., Fellers C., Nilvebrant N. Friction hysteresis of paper. *Wear* 2004, *256*, 190–196.
35. Al-Bender F., Symens W. Characterization of frictional hysteresis in ball-bearing guideways. *Wear* 2005, *258*, 1630–1642.
36. Kivelson D., Reiss H. Metastable systems in thermodynamics: consequences, role of constraints. *J. Phys. Chem. B* 1999, *103*, 8337–8343.
37. Diestler D. J., Gao G. T., Zeng X. C. Role of hysteresis in the molecular picture of friction. *Phys. Chem. Chem. Phys.* 2001, *3*, 1175–1178.
38. Diestler D. J. Constrained statistical thermodynamic treatment of friction. *J. Chem. Phys.* 2002, *117*, 3411–3423.
39. Brodsky E. E., Kanamori H. Elastohydrodynamic lubrication of faults. *J. Geophys. Res.* 2001, *106*, 16357–16374.
40. Daniels K. E., Behringer R. P. Hysteresis and competion between disorder and crystallization in sheared and vibrated granular flow. *Phys. Rev. Lett.* 2005, *94*, 168001.
41. Arcangelis L., Lippiello E., Pica Ciamarra M., Sarracino A. Induced and endogenous acoustic oscillations in granular faults. *Phil. Trans. A* 2018, *377*, 20170389.
42. Allen M. P., Tildesley D. J. *Computer Simulation of Liquids*; Clarendon: Oxford, 1987.
43. Spohr E., Heinzinger K. Molecular dynamics simulation of a water/metal interface. *Chem. Phys. Lett.* 1986, *123*, 218–221.
44. Kim H. J., Kim D. E. Water lubrication of stainless steel using reduced graphone oxide coating. *Sci. Reports* 2015, *5*, 17034.
45. Amann T., Gatti F., Li K., Demirel Y., Kailer A., Feng H., Yuan C. Investigation of ionic liquids with and without graphene as lubricant additive for metal/metal and metal/PEEK contacts over a wide temperature range. *Lub. Sci.* 2021, *33*, 100–111.
46. DeGiuli E., Wyart M. Friction law and hysteresis in granular materials. *PNAS* 2017, *114*, 9284–9289.
47. Zhuravlev V. A. On the qustion of theoretical justification of the Amontons-Coulomb law for friction of unlubricated surfaces. *J. Mech. Tribol.* 2007, *221*, 893–898.
48. Blau P. J. The significance and use of the friction coefficient. *Trib. Inter.* 2001, *34*, 585–591.

Supplementary Material: This article contains supplementary material (https://doi.org/10.1515/zpch-2023-0220).